DOI: 10.13009/EUCASS2022-4730
9TH EUROPEAN CONFERENCE FOR AERONAUTICS AND SPACE SCIENCES (EUCASS)

HyperCODA – Extension of Flow Solver CODA Towards Rocket Flows

Stefan Fechter[⋆,†] *and Immo Huismann*[§]
[⋆]*German Aerospace Center (DLR), Institute of Aerodynamics and Flow Technology*
Göttingen, Germany
[§]*German Aerospace Center (DLR), Institute of Software Methods for Product Virtualization*
Dresden, Germany
stefan.fechter@dlr.de · immo.huismann@dlr.de
[†]Corresponding author

Abstract

For the development of modern reusable rocket launch and reentry vehicles, accurate simulation is imperative throughout the whole design phase. The SpaceX Falcon 9 rocket demonstrated feasibility of reusing first and second stage of a rocket, which lowers operating costs for target-to-space operations. This led to a boom of research effort in this sector, aiming to prevent the spacecraft structures from failing during the takeoff and reentry.

For the involved aerodynamic maneuvers, it is essential to reliably and accurately estimate the maximum heat flux through the body surface during takeoff and reentry. However, high temperatures, prevalent strong shocks and, in turn, dissociation of the gas complicate matters. For these applications the DLR flow solver TAU was extended with the spacecraft extensions[4] which include suitable fluid models, shock limiters, and shock-stable flux functions to cope with these types of applications. However, TAU was designed 30 years ago. Modern computer hardware incorporates performance enhancements, such as multiple cores per socket, deep cache hierarchies with non-uniform memory access, and accelerator cards. Taking advantage of optimizations for these kinds of hardware, can significantly impact the structure of a code and a full redesign is not feasible for the legacy code base.

Thus, one European effort to improve the solver basis in Europa is based on a initiative of Airbus, DLR and ONERA to develop the next generation CFD solver CODA (short for "CFD for ONERA, DLR and Airbus"). This modularized flow solver is based on common framework and architecture of the code Flucs[11] and features finite volume as well as Discontinuous Galerkin solvers with RANS and DES turbulence models. The last four years of common solver development focused on subsonic and transonic flows around aircraft. In this flow regime only weak shocks are present and the assumption of one perfect gas as fluid model proves sufficiently accurate. In contrast, the conditions in which spacecraft engines operate are more extreme: High altitude flow conditions as well as high velocities during takeoff and reentry maneuvers need to be simulated. Mach numbers in the order of 10 or above mandate specialized flow solvers able to deal with the involved strong shocks and, in turn, high temperatures and, thus, temperature-dependent ideal gas mixture equation of states (EOS).

In a first contribution about HyperCODA[7] we validated the HyperCODA extension of the flow solver CODA for conditions at high Mach number together with a perfect gas EOS. In this contribution we extend the description using a more realistic ideal gas EOS that includes high-temperature effects. This additional physical model allows us to make quantitative comparisons of the flow solver HyperCODA to the validated flow solver TAU for representative flight conditions of spacecraft vehicles during takeoff, reentry, and landing.

The paper is organized as follows: In the first section we introduce briefly the flow solver as well as the physical models, which is followed by a validation of the solver using basic examples. Then, industry-relevant test cases are shown and the paper is closed with a short summary and outlook to further work.

1. Flow solver HyperCODA

The CFD solver framework HyperCODA aims to handle the challenges of high-velocity, high-enthalpy flows, such as they appear in, e. g., space applications. A base set of physical models tailored for aerospace applications is available in the flow solver layer jointly developed by the afore-mentioned as well as further partners under the name "CFD for ONERA, DLR and Airbus", for short: CODA. Both codes are designed such that they are part of an eco-system, fully concentrating on the core CFD capabilities while reusing already existing infrastructure as much as possible. This

DOI: 10.13009/EUCASS2022-4730

leads to a separate infrastructure layer for data structures called Flis which handles parallelism, automatic differentiation (AD) support, and interfacing to the outside world, with the latter being implemented via the FlowSimulator DataManager (FSDM).[8,16] Linear problems arising from implicit schemes and linearized equations are solved using DLR's linear solver library Spliss, as described in.[10]

A more detailed description of the underlying flow solvers as well as the basics of HyperCODA can be found in Huismann et al.[7] In this publication we focus on the extensions towards reactive flows using a flamelet combustion model and tabulated ideal gases as additional thermodynamic model. This thermodynamic assumption proved to be suitable up to the temperature of dissociation of about 6000 K and, in turn, allows to compute most space-relevant flows, solely excluding high-enthalpy reentry flows where chemical dissipation occurs.

1.1 Extension to multi-component flows using tabulated gases

HyperCODA extends CODA's implementation of the Euler, Navier-Stokes and RANS equations from the assumption of a (single) perfect gas to the consideration of gas mixtures at thermodynamic equilibrium, i. e. without the need to model chemical non-equilibrium effects as dissociation. In CODA terms, implementing these equations consists of providing the state variables and the corresponding convection and diffusion terms, e. g. for the Euler equations the state consists of a vector containing the partial densities $\rho_i = \rho Y_i$ of the N species, where the Y_i denote the mass fraction of the species, $\rho\vec{v}$ the momentum, and E the stagnation energy. The necessary thermodynamic closure is provided by a module for the ideal gas mixture description that uses temperature splines for the molar specific heat at constant pressure c_p, the molar inner energy e, the molecular viscosity μ, and the thermal conductivity λ. The thermodynamic input data is generated from a NASA spline database, described, e. g., in.[12]

$$\partial_t \begin{pmatrix} \rho_1 \\ \vdots \\ \rho_N \\ \rho\vec{v} \\ \rho E \end{pmatrix} + \nabla \cdot \begin{pmatrix} \vec{v}\rho_1 \\ \vdots \\ \vec{v}\rho_N \\ \vec{v} \otimes \rho\vec{v} + p \\ \vec{v}(\rho E + p) \end{pmatrix} = 0 \quad , \tag{1}$$

with the ideal gas mixture closure connecting pressure p, temperature T and the state:

$$p = \rho R T \tag{2}$$

$$R = \sum_{i=1}^{N} R_i Y_i, \quad c_\mathrm{v} = \sum_{i=1}^{N} c_{\mathrm{v},i}(T) Y_i \tag{3}$$

$$e = \sum_{i=1}^{N} e_i(T) Y_i \quad \text{with} \quad e_i = h_0^f + \int c_{\mathrm{v},i} dT \quad . \tag{4}$$

Here, each R_i denotes the species gas constants for species i resulting from the universal gas constant R_u and the molecular weights M_i via $R_i = R_\mathrm{u}/M_i$. h_0^f denotes the zero-point energy of formation of the species. Furthermore, the $c_{\mathrm{v},i}(T)$ denote the temperature-dependent specific heat at constant volume for the species. All temperature-dependent data is tabulated from the NASA polynomials and provided as temperature-dependent data to the solver. Fast linear operators interpolate the thermodynamic database during the solver runtime.

In contrast to a perfect gas law (using a constant specific heat ratio γ), for which an analytical formula for the pressure from the density and energy stagnation density is available, the temperature of the mixture state for an ideal gas (with non-linear energy behavior) has to be determined using an iterative method. This iteration provides the pressure and temperature from the density and the energy stagnation density and converges usually within few iterations.

For the Navier-Stokes equations for gas mixture, three diffusion terms occur on the right-hand side, one due to the shear stresses, one due to the varying species concentrations and one due to the enthalpies of the species.[4] The molecular mixture transport properties are computed from individual species contributions using the Wilke mixture rule.[19] Lastly, the RANS implementations extend the state with further variables while directly reusing convection, diffusion, and source terms from CODA.

DOI: 10.13009/EUCASS2022-4730

1.2 Extension to flamelet combustion model

One choice to include combustion effects into the flow description is to use a flamelet combustion model that idea originates back to Peters.[14] The idea is tabulate the reactive flame composition as a self-similar function of the mixture fraction Z, its variance Z'' and a scalar dissipation function χ. The solution for the reactive flame composition is obtained in a preprocessing step by solving the flamelet equations and then tabulated in a three-dimensional lookup table. Thus, it is neither necessary to solve for N species transport equations nor to solve the kinetic source terms in the solver to have the reactive composition available in the flow solver. This fact makes the flamelet model attractive for large kinetic schemes with many species involved.

Within CODA's spatial discretization this adds two transport equations, one for the mixture fraction Z, and one for its variance Z''. The scalar dissipation function χ is computed from the turbulent length scale ω and the variance of the mixture fraction Z'' as

$$\chi = C_\chi C_\mu \omega Z''^2.$$

The constants are typically chosen to $C_\chi = 2.0$ and $C_\mu = 0.09$.

The implemented flamelet combustion model assumes a Lewis number of unity, simplifying the energy diffusion term, see e. g. the description in Karl.[9] This is an appropriate approximation for the considered gaseous flows. Thus, the resulting equation system in the CFD solver to be solved is (neglecting the source terms):

$$\partial_t \begin{pmatrix} \rho \\ \rho\vec{v} \\ \rho E \\ \rho k \\ \rho\omega \\ \rho Z \\ \rho Z'' \end{pmatrix} + \nabla \cdot \begin{pmatrix} \vec{v}\rho \\ \vec{v} \otimes \rho\vec{v} + p \\ \vec{v}(\rho E + p) \\ \vec{v}\rho k \\ \vec{v}\rho\omega \\ \vec{v}\rho Z \\ \vec{v}\rho Z'' \end{pmatrix} = \begin{pmatrix} 0 \\ \nabla p + \nabla \cdot \tau \\ \nabla \cdot \tau\vec{v} + \nabla \cdot \frac{\mu}{\mathrm{Sc}} \sum_i Y_i \\ \nabla \cdot (\mu + \sigma_k \mu_t) k \\ \nabla \cdot (\mu + \sigma_\omega \mu_t) \omega \\ \nabla \cdot \frac{\mu}{\mathrm{Sc}} Z \\ \nabla \cdot \frac{\mu}{\mathrm{Sc}} \left(Z'' + (Z'')^2 \right) - \rho\chi \end{pmatrix}, \tag{5}$$

with the ideal gas closure for the N tabulated mass fractions Y_i connecting pressure p, temperature T and the state:

$$p = \rho R T \tag{6}$$

$$R = \sum_{i=1}^{N} R_i Y_i, \quad c_\mathrm{v} = \sum_{i=1}^{N} c_{\mathrm{v},i}(T) Y_i \tag{7}$$

$$e = \sum_{i=1}^{N} e_i(T) Y_i \quad \text{with} \quad e_i = h_0^f + \int_T c_{\mathrm{v},i} dT \tag{8}$$

The flamelet model requires the turbulent time scale ω as input to compute the scalar dissipation function χ. Thus, it can just be combined with a turbulence model that provides a turbulent time scale. Within the CODA context, this applies for the Menter SST turbulence model[13] as well as the Wilcox turbulence model.[18] The molecular mixture transport properties are computed from individual species contributions using the Wilke mixture rule.[19]

2. Validation test cases

This section is dedicated to the basic validation test cases as validation of the implementation of the models within HyperCODA. The first test case investigates stability at high Mach number flows while the second and third test validate the mixing implementation.

2.1 Blunt body test case

In Huismann et al.[7] this test was introduced to show the stability of the CFD code for shocks at high Mach numbers. The geometry is detailed in Figure 1 with $r = 1$ and $R = 3$ is used. The general description of this test case can be found e. g. in Quirk.[15] While the half-cylinder serves as a wall boundary, the left bound serves as inlet with $Ma_\infty = 15$ and $\rho_\infty = 1$, and the right side as outlet with $p_\infty = 1$. This domain was discretized using a structured mesh using $N_r = 160$ grid points in the radial direction and $N_\phi = 480$ in the azimuthal one.

In addition to the case study using different upwind flux solvers shown in[7] we simulate this test case here with a different thermodynamic model, i. e. with an ideal gas with a tabulated non-linear energy behavior. This is the more

DOI: 10.13009/EUCASS2022-4730

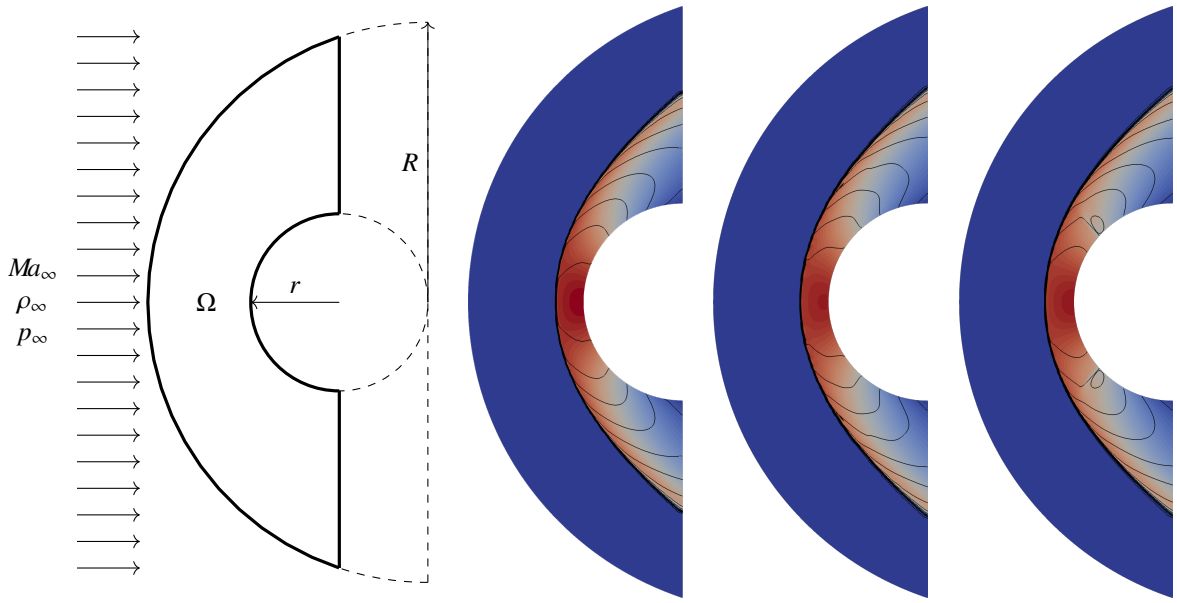

Figure 1: Left: Setup for the blunt body testcase. Bold lines bound the computational domain Ω, dashed lines are used for construction of it. Right: Simulation results for the blunt body test case at $Ma = 15$. The color corresponds to the density ρ, with blue denoting the upstream density ρ_∞ and red the stagnation density $8.8\rho_\infty$. The corresponding temperature isolines are plotted in black. From left to right: DLR TAU using AUSMDV with Carbuncle fix, HyperCODA using HLLC flux, and HyperCODA using AUSM+M.

appropriate fluid model for gases at high temperatures until the start of dissociation at temperatures of about 6000 K. Due to the strong shock in this test case the temperature of the fluid increases considerably. In all cases, constant reconstruction was employed in conjunction with an explicit time-stepping scheme and the simulations ran until their density residual was reduced by a factor of 10^{-10}. Due to the non-appropriate thermodynamic model the maximum temperature in the stagnation region is higher.

For comparison, the problem was simulated three times: First, a numerical reference solution is generated with DLR TAU, using the AUSM-DV flux including the Carbuncle fix proposed in[5] using a tabulated ideal gas for air. Second, with HyperCODA using AUSM+M[1] with the assumption of air as tabulated ideal gas, and, lastly, with the HLLC flux using the same thermodynamic model. In all cases, constant reconstruction was employed in conjunction with an explicit time-stepping scheme and the simulations ran until their density residual was reduced by a factor of 10^{-10}.

Figure 1 depicts the results of the simulations using the ideal gas model. In all simulations the numerical flux function computes the physical correct solution: A sharp, bow-shaped shock surrounds the cylinder. The so-called Carbuncle phenomenon that is dependent on the flux function and its diffusivity is suppressed in the TAU and HyperCODA computations. Note that due to the more appropriate thermodynamic model, the maximum temperature in the stagnation point is reduced resulting a more realistic estimate.

2.2 Mixing of gases in a coaxial injector setup

As first gas mixture test case we use the geometry of the two-dimensional Ruiz test case as originally proposed by Ruiz et al.[17] for cryogenic fluid mixing. The geometry represents the initial part of a coaxial injector with an oxygen core and a surrounding fuel ring simplified to a two-dimensional mesh. This generic test case is attractive as it allows for code validation at low computational costs while using a relevant geometry. The geometry and inlet conditions for the gaseous test case are described in Figure 2. The inlet conditions are modified such to have gaseous inflow conditions.

DOI: 10.13009/EUCASS2022-4730

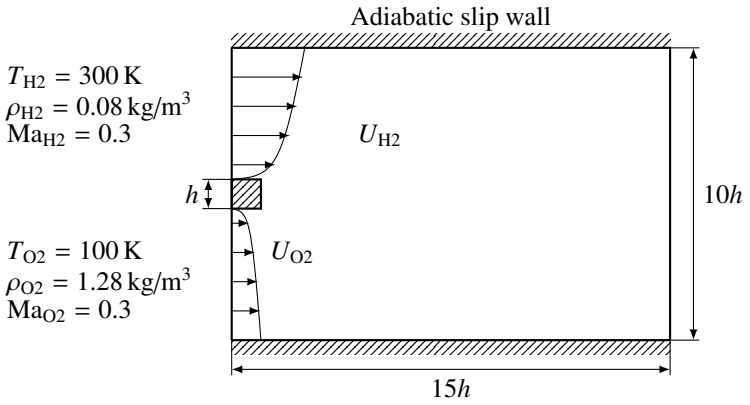

Figure 2: Sketch of the test case for Hydrogen/Oxygen mixing following the geometrical definition of the original test case proposed by Ruiz et al.[17] for cryogenic fluids.

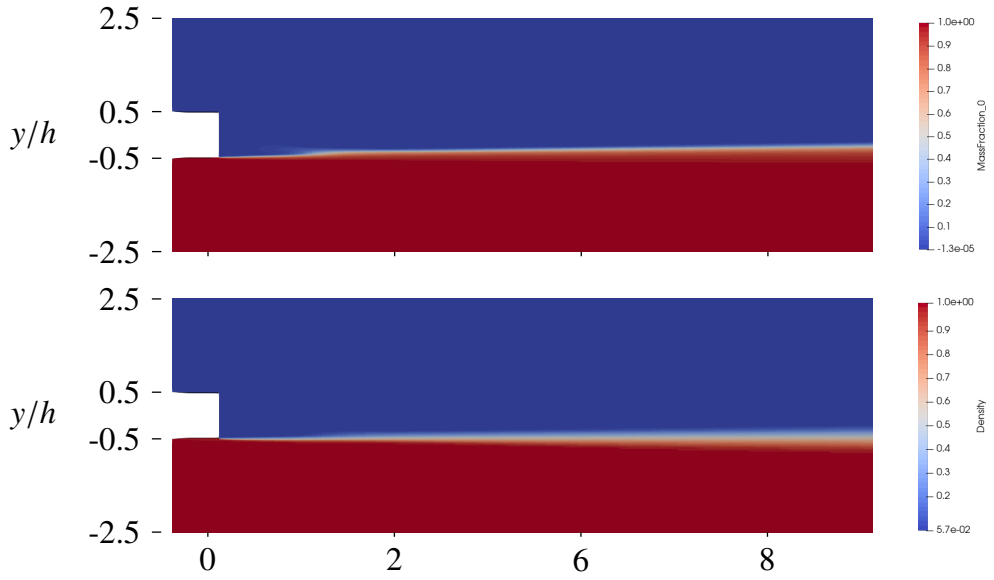

Figure 3: RANS results for the gaseous mixing of hydrogen and oxygen. From top to bottom: Top: Oxygen massfraction distribution Y_{O_2}; Bottom: Density distribution ρ/ρ_∞;

Figure 3 depicts the results attained with a RANS Wilcox turbulence model. The computed solutions make sense for a turbulent mixing layer of hydrogen and oxygen. In the flow field we see a nearly constant pressure distribution and the temperature changes are marginal. Further more detailed comparisons of the flow solution at various slides might be an additional cross-code verification.

2.3 Flamelet combustion in a coaxial injector setup

The gaseous mixing test case in Section 2.2 is extended to a reactive mixture using a Flamelet model to obtain the reactive mixture composition. Thus, now we can consider a reactive mixture of hydrogen and oxygen. Note that this test case re-samples the processes directly after a coaxial injector as widely used in combustion chambers.

The chemical kinetics are modeled using a Flamelet approach and the composition of the reactive mixture was tabulated using the oxygen-hydrogen 9 reactions kinetics with 6 species (O_2, O, H_2, H, H_2O and OH) detailed in Gerlinger.[3] Details on the flamelet tabulation process can be found in Horchler[6] for which the flamelet equations are solved and the result was tabulated in terms of the mixture fraction, its variance as well as the scalar dissipation function. Again we apply the NASA splines for the thermodynamic properties of the 6 species and use the RANS Wilcox turbulence model in HyperCODA.

DOI: 10.13009/EUCASS2022-4730

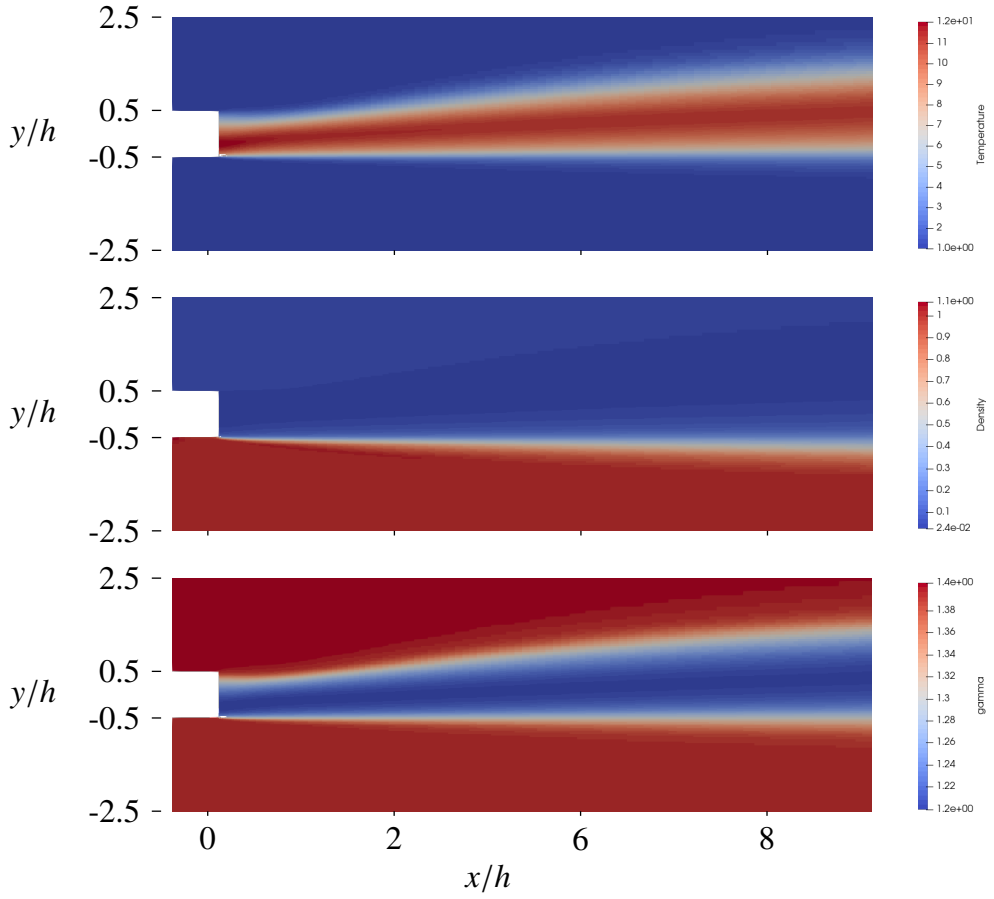

Figure 4: RANS results for the gaseous combustion of hydrogen and oxygen using a simplified hydrogen-oxygen combustion kinetics described in Gerlinger.[3] From top to bottom: Top: Temperature distribution T/T_∞; Middle: Density distribution ρ/ρ_∞; Bottom: Distribution of the adiabatic coefficient $\gamma = c_p/c_v$.

The results for the flamelet test case are plotted in Figure 4 visualizing the steady-state non-dimensional temperature, non-dimensional density and γ distribution. The dimensional reference state is given by the density $\rho_\infty = 1.2\,\mathrm{kg\,m^{-3}}$, the pressure $p_\infty = 1\,\mathrm{bar}$ and the temperature $T_\infty = 300\,\mathrm{K}$. The maximal (non-dimensional) temperature T/T_∞ is in agreement with the (tabulated) maximal flamelet temperature. The flame is anchored to the lip and the oxidizer and fuel are separated by the flame zone. Note that with the present flamelet implementation it is not possible to determine flame liftoff effects.

Due to the reactive mixture at the high temperatures the adiabatic coefficient varies substantially visualizing the necessity to treat the mixture using tabulated fluid properties.

3. Application cases: Falcon 9 retropropulsion

This section performs a cross-code comparison between DLR TAU and the HyperCODA solver framework with the retropropulsion test case described in Ecker et al.:[2] A simplified, descending Falcon 9 rocket. A cylinder with an attached 9-engine configuration represents the rocket and only three of the nine Merlin 1D+ engines are fired during the reentry maneuver. The simulation tries to recapture the trajectory point 5 in,[2] corresponding to an altitude of 25 km and a free-stream Mach number of $Ma = 2$, using the Spalart–Allmaras turbulence model. First results for the effect of retropropulsion on the flow features are shown.

The composition is evaluated at free-stream conditions for the air and at the nozzle exit for the kerosene exhaust fluid, with the properties thereof being calculated from the mean components in the nozzle based on a separate nozzle calculation described in.[2] The temperature-dependent fluid properties of the mixtures 'air' and 'exhaust' are computed based on NASA thermodynamic data[12] and mixture rules. This is the same fluid model that was used for the reference computations with TAU in.[2] Table 1 lists the constituents of the two species and their compositions. Furthermore, the frozen heat capacity ratio γ for the frozen mixture approach is detailed.

DOI: 10.13009/EUCASS2022-4730

Table 1: Thermodynamic properties of the fluids

Fluid	air		exhaust			
Species composition	N_2	O_2	CO	CO_2	H_2	H_2O
Mass fractions Y [-]	0.76	0.233	0.39	0.10	0.15	0.31
Mixture molar mass M [$^{kg}/_{mol}$]	0.02884		0.0234			
Frozen heat capacity ratio γ [-]	1.4		1.267			

With frozen fluid properties (perfect gas mixture):

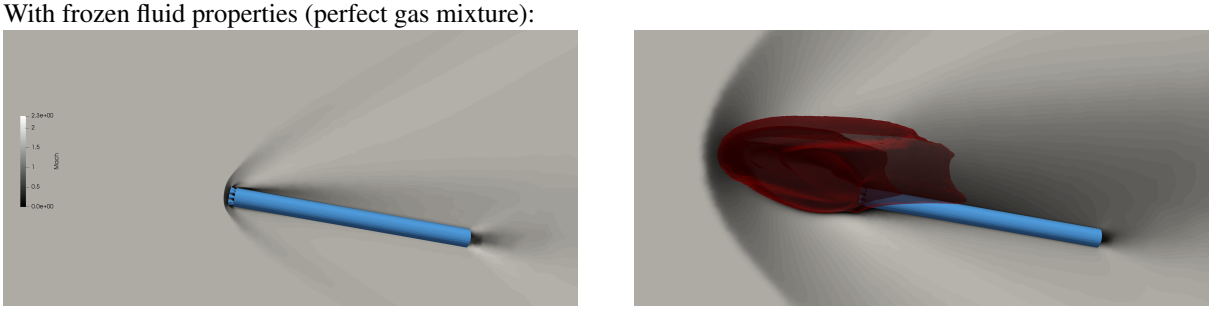

With tabulated fluid properties (ideal gas mixture):

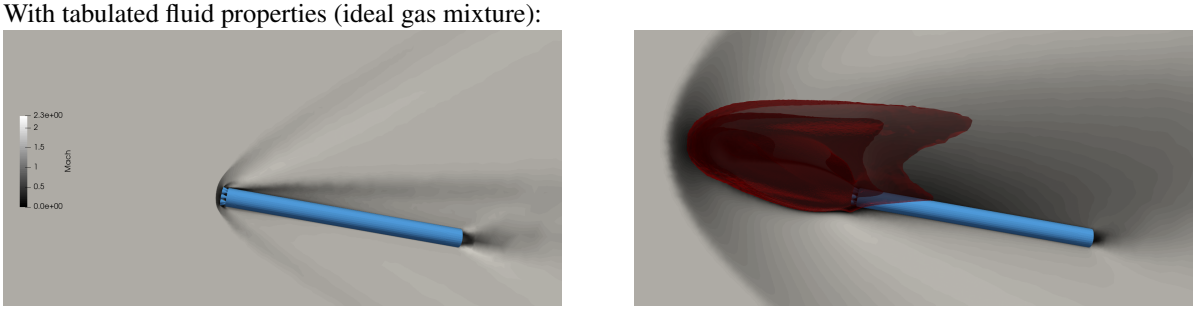

Figure 5: Comparison of Mach number distribution with 'engine off' and 'engine on' at $\alpha = 10$ deg, $h = 25$ km, and $M_\infty = 2.0$. The rocket body is highlighted in blue. Left: Simulation with engine off. Right: Simulation with 'engine on' with visualization of the plume isosurface with levels of 25, 50, and 75 % exhaust mass fractions (from inside to outside) in reddish colors.

Figure 5 visualizes the effect of the hot exhaust plume onto the Mach number distribution. Without retropropulsion, a thin shock lies very close to the rocket and an expansion wave is present on the upper side. With activated retropropulsion, the exhaust moves the shock further away from the rocket while making it stronger. Due to the effect of the plume, the expansion wave on the upper side is not present in the case of 'engine on'. The hot plume close to the rocket causes a significant heating of the structure.

Comparing the result of the frozen approximation on the top to the one using temperature-dependent fluid properties, we see an influence on the flow field for the case with 'engine on'. This is due to the reached large temperatures in the jet impinging onto the shock. For the case with 'engine off' the effects are negligible because no large temperature changes are present in the flow field.

Similar findings were reported in[2] and with HyperCODA, the main flow features could be reproduced for the advanced use case of rocket propulsion.

4. Conclusions

This paper presented recent advances within the physical modeling of the flow solver HyperCODA the extension of DLR's flow solver CODA to high-enthalpy flows and multi-species fluids. First, the joint infrastructure was shortly introduced. The more recent ideal gas mixture model of HyperCODA was verified to be a suitable candidate for simulations up to the onset of dissociation at about 6000 K). Then, the Carbuncle effects were investigated using a more suitable fluid model due to the high temperatures in the stagnation point region of the cylinder test case at a Mach number of 15. The implementation of the mixture and the flamelet combustion model were verified using a simple two-dimensional test case that is a suitable model for the core region of a coaxial injector. Lastly, a three-dimensional test

DOI: 10.13009/EUCASS2022-4730

case constituted an application of HyperCODA to three-dimensional flows to flows with retropropulsion. The results are plausible in comparison with TAU while the code base is modular, more easily verifiable and testable, and offering novel temporal and spatial discretization schemes.

The next steps consist of further validation of the code framework as well as an extension to cryogenic fluid mixtures to further address the full range of spacecraft applications.

Acknowledgements

The present work was conducted in the framework of the German Aerospace Center (DLR) project AMADEUS (Advanced Methods for Reusable Aerospace Vehicle DEsign Using Artificial Intelligence and Interdisciplinary Numerical Simulation) and COANDA (CODA-Automatisierung und -Nutzbarmachung für Diversifizierte Anwendungsfelder) with the first one focusing on the extension of the DLR flow solver CODA for liquid rocket thrust chamber applications and the latter on focusing on the extension of the CODA solver for further application areas. The financial support of the DLR Space Research Programmatic is highly appreciated.

References

[1] Shu-Sheng Chen, Fang-Jie Cai, Hai-Chao Xue, Ning Wang, and Chao Yan. An improved AUSM-family scheme with robustness and accuracy for all Mach number flows. *Applied Mathematical Modelling*, 77:1065–1081, 2020.

[2] Tobias Ecker, Sebastian Karl, Etienne Dumont, Sven Stappert, and Daniel Krause. Numerical study on the thermal loads during a supersonic rocket retropropulsion maneuver. *Journal of Spacecraft and Rockets*, 57(1):131–146, 2020.

[3] Peter Gerlinger. *Numerische Verbrennungssimulation: Effiziente numerische Simulation turbulenter Verbrennung*. Springer-Verlag, 2005.

[4] Klaus Hannemann, Jan M Schramm, Alexander Wagner, Sebastian Karl, and Volker Hannemann. A closely coupled experimental and numerical approach for hypersonic and high enthalpy flow investigations utilising the HEG shock tunnel and the DLR TAU code. Technical report, German Aerospace Center, Braunschweig (Germany), Institute of Aerodynamics and Flow Technology, 2010.

[5] Volker Hannemann. *Numerische Simulation von Stoß-Stoß-Wechselwirkungen unter Berücksichtigung von chemischen und thermischen Nichtgleichgewichtseffekten*. PhD thesis, Dt. Forschungsanstalt für Luft-und Raumfahrt, Abt. Operative Planung, 1997. In German.

[6] Tim Horchler. *Skalenauflösende Simulation der Flammen-Akustik Wechselwirkung bei resonanter und nichtresonanter Anregung in einer Experimtental-Raketenbrennkammer*. PhD thesis, Justus-Liebig-Universität Gießen, 2022. submitted.

[7] Immo Huismann, Stefan Fechter, and Tobias Leicht. HyperCODA – extension of flow solver CODA towards hypersonic flows. In Andreas Dillmann, Gerd Heller, Ewald Krämer, and Claus Wagner, editors, *New Results in Numerical and Experimental Fluid Mechanics XIII*, pages 99–109, Cham, 2021. Springer International Publishing.

[8] Immo Huismann, Lars Reimer, Severin Strobl, Jan Robert Eichstädt, Ronny Tschüter, Arne Rempke, and Gunnar Einarsson. Accelerating the FlowSimulator: Profiling and scalability analysis of an industrial-grade CFD-CSM toolchain. In *9th edition of the International Conference on Computational Methods for Coupled Problems in Science and Engineering (COUPLED PROBLEMS 2021)*, volume 9, 2021.

[9] Sebastian Karl. *Numerical investigation of a generic scramjet configuration*. PhD thesis, Technische Universität Dresden, 2011.

[10] Olaf Krzikalla, Arne Rempke, Alexander Bleh, Michael Wagner, and Thomas Gerhold. Spliss: A sparse linear system solver for transparent integration of emerging HPC technologies into CFD solvers and applications. In Andreas Dillmann, Gerd Heller, Ewald Krämer, and Claus Wagner, editors, *New Results in Numerical and Experimental Fluid Mechanics XIII*, pages 635–645, Cham, 2021. Springer International Publishing.

[11] Tobias Leicht, Jens Jägersküpper, Daniel Vollmer, Axel Schwöppe, Ralf Hartmann, Jens Fiedler, and Tobias Schlauch. DLR-project Digital-X – next generation CFD solver 'Flucs'. 2016.

DOI: 10.13009/EUCASS2022-4730

[12] Bonnie J McBride. *Coefficients for calculating thermodynamic and transport properties of individual species*, volume 4513. National Aeronautics and Space Administration, Office of Management . . . , 1993.

[13] Florian R Menter, Martin Kuntz, and Robin Langtry. Ten years of industrial experience with the sst turbulence model. *Turbulence, heat and mass transfer*, 4(1):625–632, 2003.

[14] Norbert Peters. Laminar diffusion flamelet models in non-premixed turbulent combustion. *Progress in energy and combustion science*, 10(3):319–339, 1984.

[15] James J Quirk. A contribution to the great Riemann solver debate. In *Upwind and High-Resolution Schemes*, pages 550–569. Springer, 1997.

[16] Lars Reimer. The FlowSimulator – a software framework for CFD-related multidisciplinary simulations. In *NAFEMS European Conference: Computational Fluid Dynamics (CFD) — Beyond the Solve*, 2015.

[17] Anthony M Ruiz, Guilhem Lacaze, Joseph C Oefelein, Raphael Mari, Bénédicte Cuenot, Laurent Selle, and Thierry Poinsot. Numerical benchmark for high-reynolds-number supercritical flows with large density gradients. *AIAA Journal*, 2015.

[18] David C Wilcox. Reassessment of the scale-determining equation for advanced turbulence models. *AIAA journal*, 26(11):1299–1310, 1988.

[19] CR Wilke. A viscosity equation for gas mixtures. *The journal of chemical physics*, 18(4):517–519, 1950.